J Neurophysiol
88: 991–1004, 2002; 10.1152/jn.00943.2001.

Short- and Long-Term Changes in Joint Co-Contraction Associated With Motor Learning as Revealed From Surface EMG

RIEKO OSU,[1,2] DAVID W. FRANKLIN,[2,3] HIROKO KATO,[4] HIROAKI GOMI,[5,6] KAZUHISA DOMEN,[7] TOSHINORI YOSHIOKA,[1,2] AND MITSUO KAWATO[1,2]

[1]*Kawato Dynamic Brain Project, Japan Science and Technology Corporation and* [2]*ATR Human Information Science Laboratories, Department 3, 2-2-2 Hikaridai, Soraku-gun, Kyoto 619-0288, Japan;* [3]*School of Kinesiology, Simon Fraser University, Burnaby, British V5A 1S6, Canada;* [4]*Intelligent Communication Laboratory, Nippon Telegraph and Telephone Corporation Communication Science Laboratories, 2–4 Hikaridai, Soraku-gun, Kyoto 619-0237, Japan;* [5]*Human and Information Science Laboratory, Nippon Telegraph and Telephone Corporation Communication Science Laboratories and* [6]*Core Research for the Evolutional Science and Technology Program, Japan Science and Technology Corporation 3–1 Wakamiya, Morinosato, Atsugi-city, Kanagawa-prefecture, 243-0198, Japan; and* [7]*Rehabilitation Center, Hyogo College of Medicine, Nishinomiya-city, Hyogo 663-8501, Japan*

Received 15 November 2001; accepted in final form 12 April 2002

Osu, Rieko, David W. Franklin, Hiroko Kato, Hiroaki Gomi, Kazuhisa Domen, Toshinori Yoshioka, and Mitsuo Kawato. Short- and long-term changes in joint co-contraction associated with motor learning as revealed from surface EMG. *J Neurophysiol* 88: 991–1004, 2002; 10.1152/jn.00943.2001. In the field of motor control, two hypotheses have been controversial: whether the brain acquires internal models that generate accurate motor commands, or whether the brain avoids this by using the viscoelasticity of musculoskeletal system. Recent observations on relatively low stiffness during trained movements support the existence of internal models. However, no study has revealed the decrease in viscoelasticity associated with learning that would imply improvement of internal models as well as synergy between the two hypothetical mechanisms. Previously observed decreases in electromyogram (EMG) might have other explanations, such as trajectory modifications that reduce joint torques. To circumvent such complications, we required strict trajectory control and examined only successful trials having identical trajectory and torque profiles. Subjects were asked to perform a hand movement in unison with a target moving along a specified and unusual trajectory, with shoulder and elbow in the horizontal plane at the shoulder level. To evaluate joint viscoelasticity during the learning of this movement, we proposed an index of muscle co-contraction around the joint (IMCJ). The IMCJ was defined as the summation of the absolute values of antagonistic muscle torques around the joint and computed from the linear relation between surface EMG and joint torque. The IMCJ during isometric contraction, as well as during movements, was confirmed to correlate well with joint stiffness estimated using the conventional method, i.e., applying mechanical perturbations. Accordingly, the IMCJ during the learning of the movement was computed for each joint of each trial using estimated EMG-torque relationship. At the same time, the performance error for each trial was specified as the root mean square of the distance between the target and hand at each time step over the entire trajectory. The time-series data of IMCJ and performance error were decomposed into long-term components that showed decreases in IMCJ in accordance with learning with little change in the trajectory and short-term interactions between the IMCJ and performance error. A cross-correlation analysis and impulse responses both suggested that higher IMCJs follow poor performances, and lower IMCJs follow good performances within a few successive trials. Our results support the hypothesis that viscoelasticity contributes more when internal models are inaccurate, while internal models contribute more after the completion of learning. It is demonstrated that the CNS regulates viscoelasticity on a short- and long-term basis depending on performance error and finally acquires smooth and accurate movements while maintaining stability during the entire learning process.

INTRODUCTION

Muscle and peripheral reflex loops possess springlike properties that pull joints back to equilibrium positions by generating restoring forces against external perturbations. This viscoelasticity can be regarded as the peripheral feedback control gain, which is adjustable by regulating muscle co-contraction levels and reflex gains. It has been hypothesized that by exploiting this viscoelasticity (Mussa-Ivaldi et al. 1985), the CNS can control the limbs by simply commanding a series of stable equilibrium positions aligned along the desired movement trajectory (equilibrium-point control hypothesis) (Bizzi et al. 1984; Feldman 1966; Flanagan et al. 1993; Flash 1987; Hogan 1984). This theory, however, requires that viscoelastic forces increase as the movement speeds up, because the dynamic forces acting on the multijoint links grow in rough proportion to the square of the velocity. On the other hand, the alternative hypothesis, referred to as internal model control, enables the realization of fast and accurate movements even with low viscoelastic forces. Under this hypothesis, the CNS learns internal models that simulate the dynamics of the musculoskeletal system and external environment and generates the required feedforward motor commands (Bizzi and Mussa-Ivaldi 1998; Kawato et al. 1987; Miall et al. 1993; Shidara et al. 1993).

It has been a matter of controversy whether the CNS relies

Address for reprint requests: R. Osu, ATR Human Information Science Labs, 2–2-2, Hikaridai, Seika-cho, Soraku-gun, Kyoto 619-0288, Japan (E-mail: osu@atr.co.jp).

The costs of publication of this article were defrayed in part by the payment of page charges. The article must therefore be hereby marked "*advertisement*" in accordance with 18 U.S.C. Section 1734 solely to indicate this fact.

on high viscoelastic forces without internal models or utilizes acquired internal models with low viscoelastic forces (Gomi and Kawato 1996; Gribble and Ostry 2000; Gribble et al. 1998; Katayama and Kawato 1993; Koike and Kawato 1993; Lackner and Dizio 1994; Latash and Gottlieb 1991). Recent observations on relatively low stiffness levels during well-trained movements support the existence of internal models (Bennett et al. 1992; Burdet et al. 2000, 2001; Gomi and Kawato 1996). On the other hand, reports that EMG is higher in a novel environment than a normal environment (Basmajian and De Luca 1985; Bernstein 1967; Milner and Cloutier 1993; Thoroughman and Shadmehr 1999) indirectly suggest that the viscoelasticity at the beginning of learning may not be as low as that after extensive training. In other words, the CNS may rely on viscoelastic forces more heavily at the beginning of learning when internal models are poor, and it may gradually increase the internal model contribution as learning proceeds, resulting in decreases in the viscoelasticity. Although several studies have tried to model such a dual strategy (Flash and Gurevich 1997; Gribble and Ostry 2000; Katayama et al. 1998; Wang et al. 2001), no previous experimental study has clearly proven the existence of pure decreases in viscoelastic forces that would imply improvement of internal models. The observed decrease in electromyogram (EMG) during learning in previous studies might have other explanations, such as trajectory modifications leading to reduced joint torques or lower reflex contributions due to the attenuation of external perturbations. One way to circumvent such complications is to require strict trajectory control and look only at successful trials having identical trajectory and torque profiles.

In this study, we developed a novel method to evaluate viscoelastic forces around the joint using EMG signals and inferred changes in viscoelasticity associated with learning. We also investigated short-term interactions between performance errors and viscoelastic forces by time-series analysis. Our findings suggest that the relative contributions of internal model control and viscoelasticity to the final motor command are adaptively regulated on a long-term and short-term basis.

METHODS

Experimental design

The experiments consisted of two parts. First, we proposed an index of muscle co-contraction around the joint (IMCJ) computed from surface EMG and joint torques, and compared the IMCJ with stiffness measured using the conventional method, i.e., applying mechanical perturbations (method evaluation). Then, we performed a second experiment in which we elucidated learning-associated changes in viscoelasticity using the proposed IMCJ. Six healthy subjects participated in the learning experiments (4 males and 2 females; ages 20–36 years; 1 male was left-handed). Two of the six also participated in the method evaluation experiments under the isometric condition. Three other subjects participated in the method evaluation experiment under the dynamic condition (2 males and 1 female; ages 29–34). The institutional ethics committee approved the experiments, and the subjects gave informed consent prior to participation.

Definition of the IMCJ

Gomi and Kawato (1996) and Burdet et al. (2000, 2001) measured stiffness during multijoint arm movements using a high-performance computer-controlled mechanical interface [Parallel Link Direct-Drive Air-Magnet Floating Manipulandum (PFM)] to displace the hand slightly during each movement and measure the restoring force. Unfortunately, these methods require many trials so they cannot be used to observe progressive changes in the stiffness that accompanies learning. Based on a report that the surface EMG is highly correlated with the static stiffness (Osu and Gomi 1999), and that the joint stiffness is highly correlated with the joint torque (Gomi and Osu 1998; Hunter and Kearney 1982), we propose the following index for evaluating joint stiffness, using surface EMG instead of direct measurements.

If rectified surface EMG signals are assumed to be proportional to isometric muscle tension (Basmajian and De Luca 1985), the joint torque can be expressed as the difference between the flexion torque exerted by the flexor muscles (weighted muscle tension) and the extension torque exerted by the extensor muscles

$$\tau_s = c_1u_1 - c_2u_2 + c_5u_5 - c_6u_6$$
$$\tau_e = c_3u_3 - c_4u_4 + c_7u_5 - c_8u_6 \quad (1)$$

Here, τ_s and τ_e denote the shoulder joint torque and elbow joint torque, respectively. u_i denotes an individual muscle activity, which is assumed to be proportional to the rectified and averaged surface EMG signals. u_1 and u_2 denote the activity of shoulder monoarticular flexor and extensor muscles, u_3 and u_4 denote the activity of elbow monoarticular flexor and extensor muscles, and u_5 and u_6 denote the activity of biarticular flexor and extensor muscles. The parameters c_i include both the moment arm and conversion factor from the muscle activity (rectified and averaged EMG) to muscle tension. The parameters c_i are all constants, as long as the moment arm is assumed to be constant. Supposing that each muscle stiffness term is proportional to the corresponding muscle torque (weighted muscle tension; c_iu_i in *Eq.1*) (Gomi and Osu 1998; Hunter and Kearney 1982), we may be able to use the summation of muscle torques as a measure for the joint stiffness. Therefore we define IMCJ as follows

$$S_s = c_1u_1 + c_2u_2 + c_5u_5 + c_6u_6$$
$$S_e = c_3u_3 + c_4u_4 + c_7u_5 + c_8u_6 \quad (2)$$

Here, S_s and S_e denote the IMCJ at the shoulder and elbow, respectively. Simultaneous increases in antagonistic muscle torques do not increase the joint torque (*Eq.1*), but do increase the IMCJs because the IMCJs are the summations of the absolute values of antagonistic muscle torques (*Eq.2*).

At a given level of activity, muscle tension nonlinearly depends on length and velocity. Accordingly, muscle stiffness also depends on length and velocity (Winters 1990), which means that surface EMG does not linearly correlate with dynamic stiffness. Further, moment arms of some muscles (e.g., pectoralis major, posterior deltoid, and brachioradialis) change during movements (Kuechle et al. 1997; Murray et al. 1995; Winters 1990). However, we assumed linear length-tension, velocity-tension curves, and constant moment arms, and approximated dynamic muscle stiffness by the weighted summation of muscle activities using parameters c_i, estimated by isometric tasks. Although these simplifications were obviously wrong and might have caused error, the error was the same for each identical movement during learning and therefore it was possible to quantify changes in stiffness across time.

The validity of the IMCJ proposed above was assessed by the following experiments under both isometric and dynamic conditions.

Evaluation of IMCJ as a good measure of stiffness

For the evaluation using isometric tasks, the subjects gripped the handle of a force sensor and were instructed to produce a specified force (0, 5, or 10 N) in a specified direction (16 directions in the hand's *x-y* plane at even intervals) without co-contraction (Fig. 1*A*). The current force vector applied by the hand to the handle and a small cross indicating the target force were displayed on a computer mon-

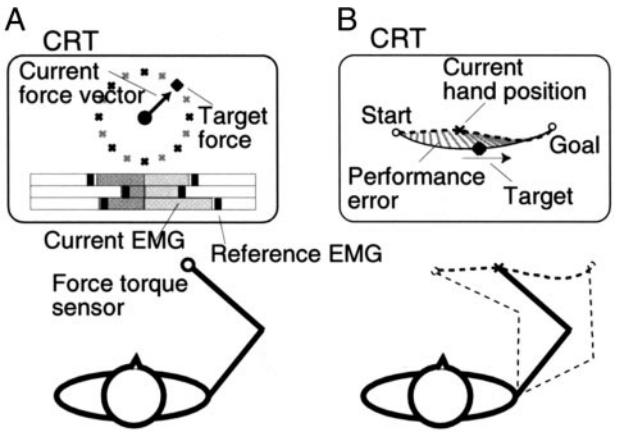

FIG. 1. *A*: experimental setup for estimating the electromyogram (EMG)-torque relationship. *B*: experimental setup. Dotted curve connecting the start position and target position denotes an actual trajectory, and the solid curve denotes a target trajectory. Performance error was determined as the root mean square of the distance between the hand and target position at each time step (the mean of the lengths of the gray lines).

itor. The right forearm of the subjects was fixed to a molded plastic cuff tightly coupled to the handle and supported in the gravity direction by a beam. The wrist joint of the subjects was fixed by the cuff, and only shoulder and elbow joint rotations in the horizontal plane were permitted. During the experiment, each subject's hand was kept at the coordinate of $[x,y] = [0.0,0.35]$ m. The subjects were required to keep the head of the force vector on the target during each experimental set to preserve the constant external force. Additionally, rectified and filtered surface EMG signals (moving average, 0.5 s) of six muscles were displayed in a bar graph. A reference line was marked on the EMG bar graph. The reference line consisted of the rectified and filtered surface EMG signals of six muscles that were determined by requesting target force exertion before each experimental set. The subjects were also asked to keep the EMG bar graph the same as the reference line so that the muscle activity would be constant during each set. The stiffness was measured at the same time by applying small perturbations using the PFM. The hand was slightly pushed and pulled back in eight randomized directions within a brief period (6–8 mm, 0.3 s, 8 directions, 3 times for each set). The subjects were asked not to intervene voluntarily during the perturbations. The details of the arm-impedance estimation method are provided elsewhere (Gomi and Kawato 1995, 1997; Gomi and Osu 1998).

The EMG was recorded from a shoulder monoarticular flexor (pectoralis major) and extensor (posterior deltoid), an elbow monoarticular flexor (brachioradialis) and extensor (lateral head of triceps brachii), and a biarticular flexor (biceps brachii) and extensor (long head of triceps brachii). The EMG signals were recorded using pairs of silver-silver chloride surface electrodes in a bipolar configuration. Each signal was filtered [cutoff frequency, 25 Hz (low) and 1,500 Hz (high)] and sampled at 2,000 Hz. The EMG signals were rectified and averaged for a period of 0.4 s before perturbations. This rectified and averaged EMG was used as muscle activity u_i in *Eq.1*. The force exerted by the hand was measured by a force sensor attached to the handle. The measured force was averaged for a period of 0.4 s. The joint torque was calculated from the average force using a Jacobian matrix.

The joint torque was decomposed into muscle torques using parameters estimated from a linear regression of the joint torque and measured EMG u_i (*Eq. 1*). All of the parameters c_i were estimated by the least-square-error method. Then, each IMCJ was computed by summing all the absolute values of flexor muscle torques and the absolute values of extensor muscle torques related to each joint (*Eq. 2*). The computed IMCJs were compared with the stiffness measured at the same time by applying perturbations (PFM-measured stiffness). We estimated linear relationships between the PFM-measured stiffness ([Nm/rad]) and the IMCJs ([Nm]) using the acquired data so we could convert the IMCJ unit to stiffness unit (rIMCJ).

Because the approximation of dynamic stiffness using IMCJ relies on oversimplified assumptions such as constant moment arms, linear length-tension, and velocity-tension curves, we evaluated whether IMCJ is still applicable for the movement data despite these simplifications. We compared IMCJ, computed by applying isometric torque-EMG relationship to dynamic EMG, to dynamic stiffness measured simultaneously. To confirm that the IMCJ represents dynamic stiffness, it is important to obtain a wide variety of stiffness estimates. However, estimating a single dynamic stiffness requires many more trials than estimating a static stiffness. To acquire enough variety of stiffness values, we used data from three subjects across three tasks measured on different days. Each subject learned three different force-fields (null force-field, velocity-dependent force-field, and position-dependent force-field) on different days. Before learning each force-field, the isometric torque-EMG relationships were measured to estimate parameters c_i in the same way as described above except that no perturbation was given. Then, subjects performed horizontal point-to-point movement away from the body in one of the three force-fields. After enough training, stiffness during the movements was measured by applying small positional perturbation to the hand (Burdet et al. 2000). At the same time, EMG signals were recorded from six arm muscles, and the corresponding shoulder and elbow IMCJs were computed using the estimated parameters c_i. Each dynamic stiffness was compared with the corresponding IMCJ. See APPENDIX 2 for details.

Learning experiments

Six subjects participated in the learning experiments. The learning experiments themselves consisted of three parts. Prior to the learning task, the subjects executed isometric contraction tasks, enabling us to estimate the relationship between the surface EMG and joint torque (parameters c_i in *Eq.1*) for the calculation of the IMCJs. Then, the subjects learned reaching movements under strict trajectory control. After the learning task, the subjects executed isometric contraction tasks again to confirm that the state of the electrodes after the learning was not different from that before the learning. From this, we confirmed that the electrode interface was not responsible for the observed changes in the surface EMG.

In the isometric contraction tasks prior to and following the learning task, each subject's hand was coupled to a force-torque sensor. The subject was instructed to produce a specified force (0, 5, 10, or 15 N for the prelearning trials and 0 or 10 N for the postlearning trials) in a specified direction (16 directions). The hand position and the instructions were the same as in the method evaluation experiment except that no perturbation was given. The hand force and EMG signals were recorded in the same way as in the method evaluation experiments.

In the learning task, the subjects performed reaching movements with the shoulder and elbow in the horizontal plane at the shoulder level. Wrist movements were constrained by a brace. The learning task consisted of moving the hand in unison with a target moving along a specified trajectory (Fig. 1*B*). The specified trajectory was curved inward, which was opposite to the natural curvature of spontaneous movements (Nakano et al. 1999). The average of 20 trials of the subject's own hand trajectory conforming to a 3.5-cm-wide inwardly curved path, performed during practice, was shifted 5 cm away and used as the target trajectory (no constraint on time was given during these preparatory 20 trials). The hand start position and end position, which were shifted away from the original average trajectory, were located at $[x,y] = [-0.24,0.37]$ m and at $[x,y] = [0.21,0.39]$ m, respectively, i.e., a movement of about 0.5 m performed in approximately 0.5 s.

Obviously, the execution of such an unusual trajectory with a strict

time course requires learning. The applied shift from the original average trajectory also enhanced the requirement of learning. To ensure that the subject would learn the accurate geometry and time course of the target trajectory, only the hand trajectories close to the target trajectory (<4 cm at each time step) were regarded as successful trials. These operations enabled us to acquire movements having identical trajectory and torque profiles both at the beginning and at the end of learning, which was necessary to prove the existence of pure decreases in the viscoelasticity and implies improvement of internal models. The current hand and target positions were displayed on a CRT. After each trial, feedback of the resulting movement was provided to the subject by replaying the target and hand movements on the CRT, providing temporal and positional error information. Hand positions within 4 cm or over 4 cm from the target were displayed in different colors so that the subject could learn his/her weak points. The performance error for each trial was specified as the root mean square of the distance between the target position and the actual hand position at each time step over the entire trajectory. The number of trials required was 96–120. Position data were acquired using the OPTOTRAK system. Surface EMG signals were recorded from six muscles involved in shoulder and elbow movements in the same way as in the method evaluation experiment.

Computation of dynamic torque

The position data obtained during the learning trials were digitally filtered by a fourth-order Butterworth filter with an upper cutoff frequency of 10 Hz. Derivatives of the position data were calculated by successively applying a three-point local polynomial approximation. Ballistic components of the movements were extracted using the curvature as a threshold to determine the beginning and the end of each movement [500 (1/m)] (Pollick and Ishimura 1996). Dynamic torques were calculated through the dynamics equation of a two-joint arm model using the position data and link parameters estimated from the link length for each subject (the data of an adult man's arm measured with a 3-dimensional scanner as a standard). The mass of the links was adjusted for each subject by changing the standard value proportional to the link length of the subject. The inertia moment of the links was adjusted by changing the standard value proportional to the third power of the link length of the subject. Viscosity coefficients were estimated from the absolute average torque for each movement using the equation in Gomi and Osu (1998). We averaged the absolute dynamic torques across whole movement durations determined by curvature criteria (average dynamic torque).

IMCJ during learning

Since IMCJs were correlated with the PFM-measured stiffness during isometric contraction tasks and dynamic tasks (see RESULTS), we calculated the IMCJ during the learning of movements. First, parameters c_i in *Eq.1* were estimated for each subject from the EMG signals and joint torques in the isometric contraction tasks executed before the learning of the movements. The EMG signals during the movements were rectified and averaged across the entire movement duration determined by curvature criteria for each muscle. Further, to roughly examine which part of each movement duration is responsible for the change, each movement duration determined by the curvature criteria was divided into the first half and the latter half, and the EMG signals were rectified and averaged over either the first half or the latter half of each movement duration. Then, the estimated parameters c_i were applied to the rectified and averaged EMG signals during movements u_i to compute the average torques of individual muscles ($c_i u_i$). The IMCJs of the shoulder and elbow were computed as the summations of the average absolute torques of individual muscles according to *Eq. 2*.

Because the parameters c_i were computed from isometric data and do not take into account the changing moment arm or velocity-tension relation, they do not accurately reproduce muscle torque during movements. The EMG signals required to generate certain muscle torques were larger during the movements than during the isometric contraction, probably due to muscle tension-shortening-velocity characteristics. Accordingly, the IMCJs during the movements computed from isometric EMG-torque relationships were corrected according to EMG-torque relationships during the movements. Namely, IMCJs were scaled based on the ratio of dynamic torque to EMG-estimated torque. The dynamic torque was, as described above, computed from actual movement trajectories using an arm inverse dynamics model and then rectified and averaged (average dynamic torques). The EMG-estimated torque was computed according to *Eq.1* by applying the isometric EMG-torque relationship (c_i) to the EMG during the movements (u_i) and rectified and averaged in the same way as the absolute dynamic torque. The correction for the movements from the isometric condition was made for each joint of each subject. We further re-scaled IMCJ by converting the unit of IMCJ ([Nm]) to the unit of stiffness ([Nm/rad]), using a linear relationship between the PFM-measured stiffness and the IMCJ estimated in the method evaluation experiment (rIMCJ).

No matter how strictly we constrained the movements, the joint torque might have slightly differed from trial to trial, which might contribute to the stiffness values (Gomi and Osu 1998). To extract the rIMCJ independent of the joint torque that implies improvement of internal models, we subtracted the torque-dependent components from the rIMCJ. Assuming that the average rIMCJ was linearly dependent on the average dynamic torque, we expressed the average rIMCJ as the summation of the weighted average dynamic torque, a constant, and residuals that could not be explained by the joint torque. The parameters (the weight and the constant) were linearly estimated by the least square error method. Then, the torque dependent components were subtracted from the rIMCJ. We called this residual component the torque-independent rIMCJ.

Bayesian multivariate feedback model for statistical analysis of time-series data

Progressive changes in viscoelasticity and performance error may be described by a dynamical system with stochastic noises. To examine the properties of the system, we can apply time-series analysis to the rIMCJ and performance error during learning. To draw inferences from the time-series data, we need to select a suitable hypothetical model to represent the data. Having chosen a model, it becomes possible to estimate parameters and use the fitted model to enhance our understanding of the mechanism generating the series. Accordingly, we set up a statistical model whose structure was designed assuming interactions between viscoelastic force and performance error (Fig. 2).

The observed rIMCJ and performance error at a certain trial number were assumed to consist of the following three components: *1*) a smooth and long-term change in the mean level of the rIMCJ and performance error, expressing a gradual decrease with the progress of learning (nonstationary trend components); *2*) short-term fluctuating components depending on previous trials, describing interactions between rIMCJ and performance error and able to be expressed as an auto-regressive (AR) model (cyclical components); and *3*) observation noise. The rIMCJ and performance error can be expressed as follows

$$R(n) = r(n) + t_r(n) + \omega_r(n) \quad \omega_r \sim N(0,10^{-4}) \tag{3}$$

$$E(n) = e(n) + t_e(n) + \omega_e(n) \quad \omega_e \sim N(0,10^{-4}) \tag{4}$$

Here, n ($1 \leq n \leq N$) denotes the current trial number. Current rIMCJ $R(n)$ is composed of cyclical component $r(n)$, trend component $t_r(n)$, and observation noise $\omega_r(n)$. Current performance error $E(n)$ is composed of cyclical component $e(n)$, trend component $t_e(n)$, and obser-

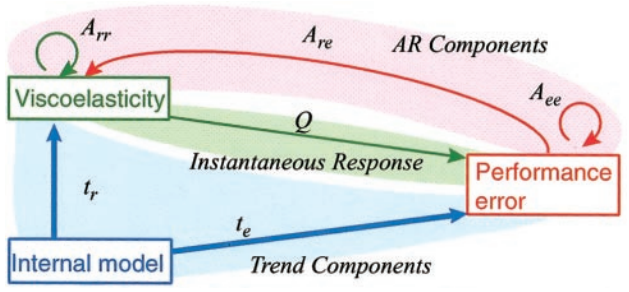

FIG. 2. Statistical model whose structure was designed assuming interactions between viscoelasticity and performance error. See the text for details.

vation noise $\omega_e(n)$. $N(m, \sigma^2)$ is the normal distribution with mean m and variance σ^2. Trend components are modeled in the form of the following second-order stochastic difference equations

$$t_r(n) = 2 \cdot t_r(n-1) - t_r(n-2) + \varepsilon_{tr}(n) \quad \varepsilon_{tr} \sim N(0, \sigma_{tr}^2) \tag{5}$$

$$t_e(n) = 2 \cdot t_e(n-1) - t_e(n-2) + \varepsilon_{te}(n) \quad \varepsilon_{te} \sim N(0, \sigma_{te}^2) \tag{6}$$

Here, $\varepsilon_{tr}(n)$ and $\varepsilon_{te}(n)$ denote system noise. The order of the two is selected to extract low-frequency components as the mean-nonstationary trends.

The following information regarding the short-term interaction between the rIMCJ and performance error was incorporated into the model describing cyclical components: *1*) current rIMCJ may change according to the performance errors in the previous trials (feedback from performance error to rIMCJ), and *2*) A high rIMCJ is assumed to decrease the current performance error but is unlikely to have an effect on subsequent performance errors (instantaneous response of performance error to rIMCJ). Therefore the cyclical components in *Eqs.3* and *4* are described by the following special form of a multivariate auto-regressive model allowing instantaneous responses

$$r(n) = \sum_{m=1}^{M} A_{rr}(m) r(n-m) + \sum_{m=1}^{M} A_{re}(m) e(n-m) + \varepsilon_r(n) \quad \varepsilon_r \sim N(0, \sigma_r^2) \tag{7}$$

$$e(n) = Q \cdot r(n) + \sum_{m=1}^{M} A_{ee}(m) e(n-m) + \varepsilon_e(n) \quad \varepsilon_e \sim N(0, \sigma_e^2) \tag{8}$$

Here, $r(n)$ is assumed to depend on the rIMCJ, performance errors of the previous M trials $[r(n-m), e(n-m), 1 \le m \le M]$, and system noise $\varepsilon_r(n)$. $e(n)$ is assumed to decrease with current rIMCJ $[Q \times r(n), Q < 0]$ and to depend on the performance errors of the previous M trials $[e(n-m), 1 \le m \le M]$ and system noise $\varepsilon_e(n)$.

This model is formulated as an extended Bayesian multivariate feedback (BMF) model (Kato and Kawahara 1998; APPENDIX 1). For the system analysis, the special form of the cyclical components was transformed into an ordinary form of a multivariate AR (MAR) model under the assumption that the noise sequences are mutually independent. This model can be represented in state space form and a Kalman filter algorithm can be applied to calculate the likelihood of the model. Parameters A_{rr}, A_{re}, A_{ee}, Q, σ_r, σ_e, σ_{tr}, and σ_{te} were estimated by the maximum likelihood method for each subject (Ishiguro and Akaike 1989). The order M of the model was selected by Akaike's Information Criterion (AIC) (Akaike 1974).

The impulse responses of the system enable us to describe how the performance error and rIMCJ interact with each other. The response of the rIMCJ obtained by providing a unit impulse input to a performance error reveals how the CNS utilizes the information of previous performance levels to modify a subsequent rIMCJ. The impulse responses of the model were calculated based on estimated model parameters (Akaike and Nakagawa 1972; Ishiguro et al. 1999).

The reliability of the estimated parameters of the model was confirmed by reapplying the system analysis to the simulated data sets, which were themselves generated based on the estimated model (Monte Carlo simulation, see APPENDIX 1).

RESULTS

High correlation between measured stiffness and IMCJ

We confirmed that the IMCJs were actually linearly correlated with the stiffness measured directly by applying mechanical perturbations (PFM-measured stiffness) during isometric force regulation tasks. We first confirmed that the joint torque could be linearly reconstructed from EMG signals in accordance with our previous studies (Gomi and Osu 1998; Osu and Gomi 1999). Figure 3*A* compares the measured joint torque and joint torque reconstructed from EMG signals of subject H.S. The coefficients of determination for the two subjects were 0.976 and 0.971. Therefore, first of all, the joint torque was well predicted from EMG signals. Then, IMCJs were computed as the summations of absolute torques of individual muscles (*Eq.2*). Figure 3*B* shows the relationship between the PFM-measured joint stiffness and corresponding IMCJ for both subjects. The open circles denote shoulder joint stiffness and the crosses denote elbow joint stiffness. The thin marks denote data from subject Y.K. and the thick marks denote data

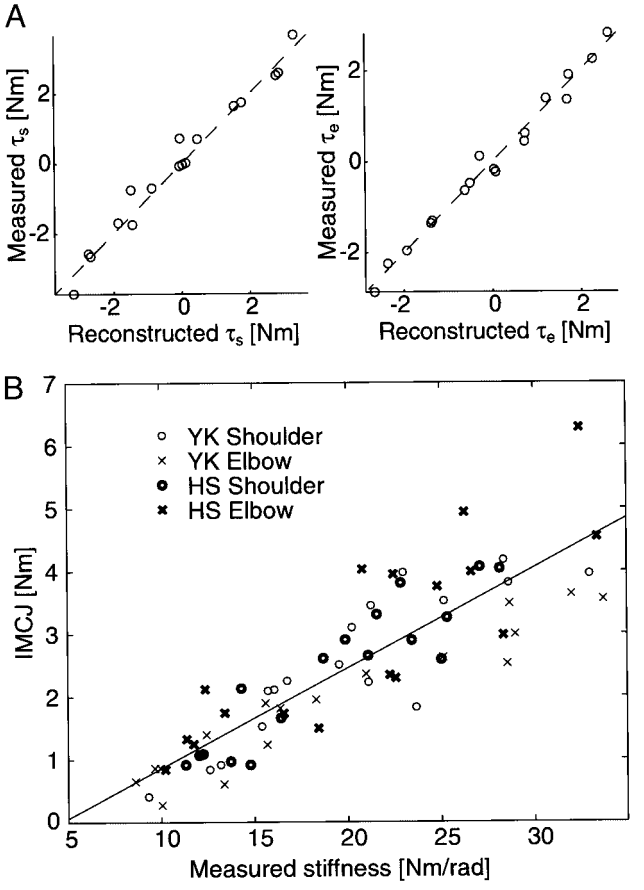

FIG. 3. *A*: regression results for subject H.S. Horizontal axis denotes the joint torque predicted from *Eq. 1*, and the vertical axis denotes the measured joint torque. *Left*: shoulder torque; *right*: elbow torque. *B*: relationship between the joint stiffness of the shoulder and elbow measured using perturbations (horizontal axis) and the corresponding index of muscle co-contraction around the joint (IMCJ) (vertical axis) for subjects Y.K. and H.S. The open circles denote the shoulder joint stiffness and the crosses denote the elbow joint stiffness.

from subject H.S. A linear relationship was observed between the IMCJs and PFM-measured joint stiffness. The correlation coefficients for the two subjects were 0.891 and 0.882. These results suggested that the IMCJ can closely predict the magnitude of the joint stiffness. The following linear relationship between the IMCJs and joint stiffness was estimated by using the least square error method. Because the relationships between the IMCJs and PFM-measured joint stiffness were similar for both the shoulder and elbow of both subjects, the slope and the intercept were estimated using all of the data

$$\text{rIMCJ ([Nm/rad])} = 6.27 \cdot \text{IMCJ ([Nm])} + 4.61$$

IMCJs ([Nm]) during learning movements were converted into rIMCJs ([Nm/rad]) using the above linear relationship. Note that the IMCJs were corrected for movements from the isometric condition for each joint of each subject before the conversion to rIMCJs, as explained in METHODS.

We also confirmed that the IMCJ is applicable for the dynamic condition. Figure 4 compares joint stiffness and the corresponding IMCJ. Each asterisk represents a value from one of the three subjects under one of the three force-fields. Even across subjects and tasks, we still observed good linear relationships between IMCJ and dynamic stiffness ($r = 0.85$ for shoulder and 0.78 for elbow). We may suppose that, if the measurements were limited to the same day and the same subjects, the reliability of the IMCJ would be even better than the results obtained here. At least within similar movement trajectories, the current method works well to quantify the relative change of joint co-contraction during the dynamic condition.

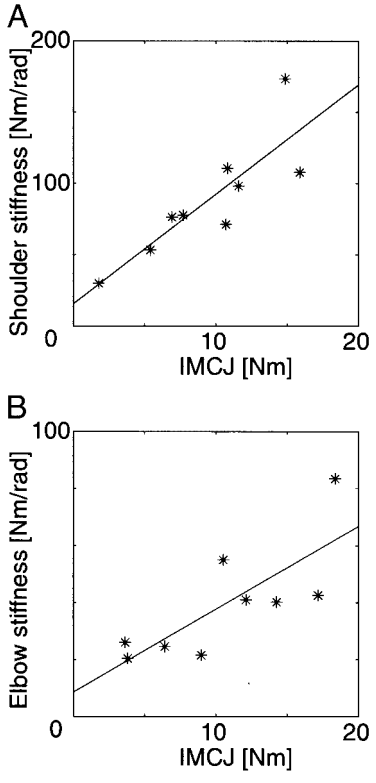

FIG. 4. *A* and *B*: relationship between the IMCJ of the shoulder (*A*) and elbow (*B*) (horizontal axis) and the corresponding joint stiffness measured using perturbations (vertical axis) during movements.

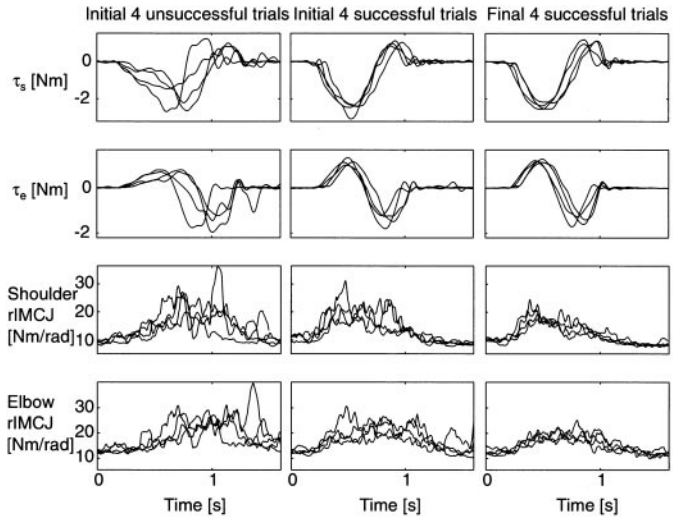

FIG. 5. Changes in the profiles of the joint torque and rIMCJ for subject Y.M. From *top* to *bottom* are the shoulder and elbow torques (τ_s, τ_e) and shoulder and elbow rIMCJs (S_s, S_e). From *left* to *right* are the initial 4 trials (all unsuccessful), the initial 4 successful trials, and the final 4 successful trials.

Invariant EMG-torque relationships before and after learning

As each experiment took a few hours, the impedance of the electrode interface might have changed with the passing of time. To verify that changes in the electrode interface were not responsible for observed changes in the surface EMG, we compared the relationships between the EMG levels and torques in the isometric contraction tasks prior to learning with those after learning for each subject. If the EMG levels in exerting the same joint torques were considerably lower after learning than before learning, the decreases in the EMG observed during the learning could not be ascribed to the effects of the learning. Fortunately, the observed EMG-torque relationships after learning were not detectably different from those before learning for any subject. The joint torque could be reconstructed from the EMG in isometric contraction tasks after learning by using the parameters estimated from the EMG-torque relationships before learning. The coefficient of determination for the seven subjects was 0.923 ± 0.059 (SD). The slope of the regression line for the seven subjects was 1.008 ± 0.099. The high coefficients of determination and the slope values close to one suggested that the relationships between the torques and EMG levels were preserved even after extensive trials. Therefore the observed decreases in the EMG levels after learning could not be ascribed to the long-term changes of the electrode state or muscle fatigue.

Long-term decrease of rIMCJ

Figure 5 shows the changes in the joint torque and rIMCJ time profiles during learning for subject Y.M. The first and second rows show the shoulder and elbow torques, respectively. The torques were calculated using the dynamics equation of a two-joint arm model. The third and fourth rows show shoulder and elbow moving-averaged rIMCJ respectively. The moving-averaged rIMCJ was calculated by applying estimated parameters c_i to EMG signals that were rectified and averaged using a 0.1-s moving-average window. The left column shows

the profiles of the initial four trials, which were all unsuccessful; the middle column shows the profiles of the initial four successful trials (early stage of learning); and the right column shows the profiles of the final four successful trials (late stage of learning). At the very beginning of the learning, the subjects failed to meet the task requirements, and as a result, their torque profiles were variable from trial to trial. However, even at the early stage of learning, the subjects soon managed to achieve several successful trials. The torque profiles of these initial successful trials were nearly identical to the torque profiles of the final successful trials. The applied strict constraint on the trajectory worked well to acquire rIMCJ data with similar torque profiles. As shown by the profiles, the rIMCJ in the successful trials decreased although the changes in the torque profiles were small. The decreases in the rIMCJ were more evident in the latter half of each movement duration.

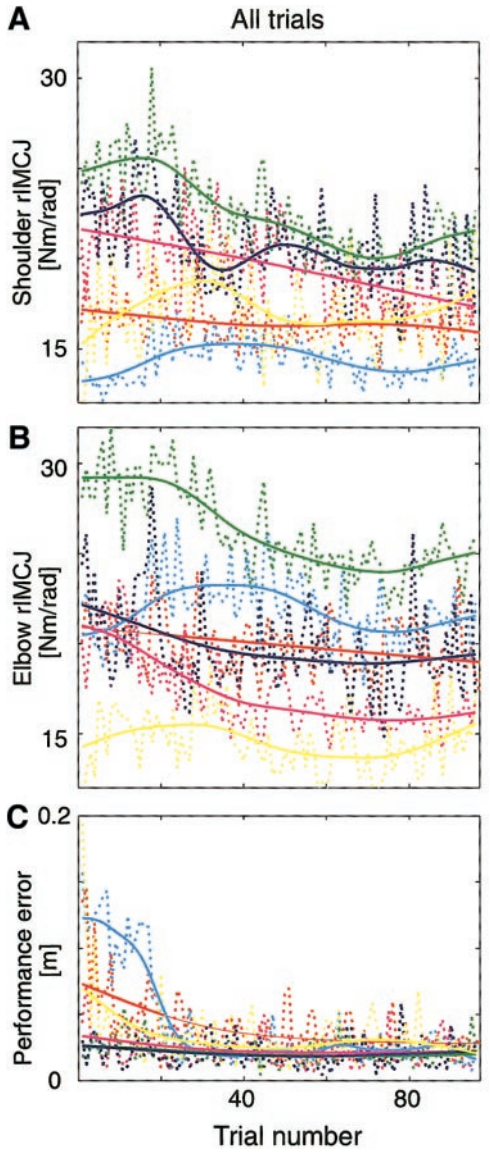

FIG. 6. *A–C*: (*A*) Shoulder and (*B*) elbow rIMCJs and (*C*) performance error across all trials for each subject. Each color corresponds to a subject (subject Y.O., magenta; subject K.D., green; subject N.H., cyan; subject H.S., blue; subject Y.K., yellow; subject Y.M., red).

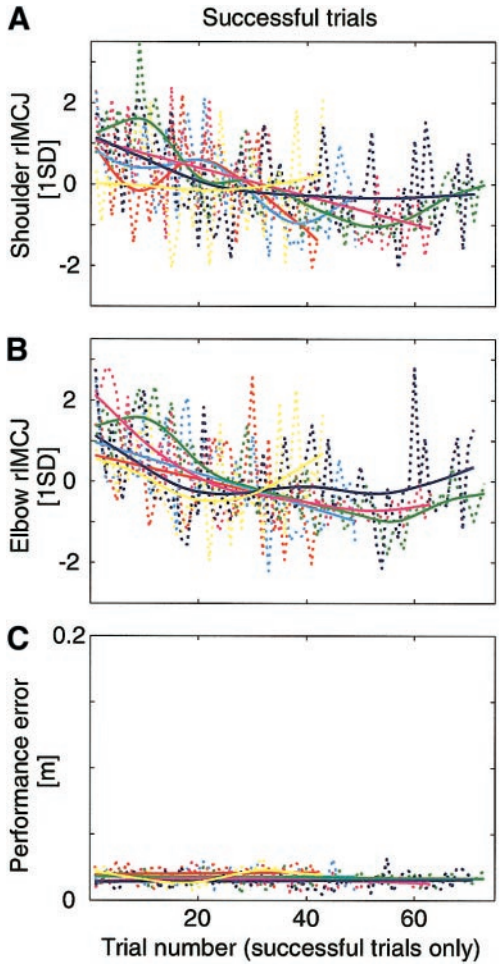

FIG. 7. *A–C*: (*A*) Shoulder and (*B*) elbow rIMCJs and (*C*) performance error across successful trials normalized for each subject (*z* score: mean 0, SD 1). Each color corresponds to a subject (subject Y.O., magenta; subject K.D., green; subject N.H., cyan; subject H.S., blue; subject Y.K., yellow; subject Y.M., red).

Figure 6, *A–C*, shows changes in shoulder and elbow rIMCJ and performance errors accompanying learning, averaged across the entire movement duration. Each color corresponds to a subject (Y.O., magenta; K.D., green; N.H., cyan; H.S., blue; Y.K., yellow; Y.M., red). The solid curves denote trend components extracted by applying the second-order trend-component model expressed in *Eqs. 5* and *6*. Both the rIMCJ and performance errors fluctuated in the short term. In four of five subjects, the mean levels of rIMCJ for both shoulder and elbow gradually decreased as the learning proceeded. For the other two subjects (N.H. and Y.K.), the mean levels of rIMCJ were rather low at the beginning of learning, but at the same time, the performance errors were comparatively large. For these subjects, the hand fell short of the target at the beginning of the learning, resulting in smaller rIMCJs with larger performance errors.

Figure 7, *A* and *B*, shows relative changes in shoulder and elbow rIMCJ in successful trials (dotted curves), with the superimposed trends (solid curves) extracted by applying the second-order trend component model. Because the magnitude of rIMCJ was different between subjects, it was normalized for each subject to 0 mean and 1 SD. Each color corresponds to a subject. Figure 7*C* shows performance errors in successful trials (dotted curves) with the trends (solid curves). As ex-

pected, the performance errors were small and nearly constant and identical for all successful trials. Because of individual differences in performance, the number of successful trials were different between subjects. The success rate of each subject was 70% for Y.O., 81% for K.D., 54% for N.H., 79% for H.S., 48% for Y.K., and 35% for Y.M. In these successful trials, every subject showed a negative correlation between the trial number and rIMCJ except for one subject (Y.K., denoted in yellow). Even for subject N.H. (denoted in blue), who showed an increase in rIMCJ at the beginning of the learning, rIMCJ for successful trials showed a significant decrease in both shoulder and elbow. The results suggest that the rIMCJ decreased with little change in the performance error.

Table 1 shows correlation coefficients between the successful trial number and the average torque-independent rIMCJ (see METHODS for definition). For the shoulder joint, five of six subjects showed a significant negative correlation between the trial number and rIMCJ. For the elbow joint, four of six subjects showed a significant negative correlation between the trial number and rIMCJ. Therefore, for the majority of the subjects and joints, the rIMCJ was found to decrease with learning independent of the joint torque. Consequently, learning enabled the generation of similar trajectories with less contribution from the viscoelasticity.

Short-term interaction between rIMCJ and performance error

As shown in Fig. 6, both the rIMCJ and performance error went up and down frequently throughout the learning process. Looking at the figure, these fluctuations appear to be simple white noise, but they might have some temporal interactions. They might reflect some dynamic system underlying the learning process. To examine the temporal relationship between the rIMCJ and performance error, the cross-correlation was computed according to the following deterministic cross-correlation sequence. The values were normalized so that, for an autocorrelation, the sample at zero lag would be 1.0

$$C_{er}(m) = \sum_{n=1}^{N-|m|} e(n)r(n+m) \tag{9}$$

Here, N denotes the total number of the trials, and m denotes the lag in the trial number between the rIMCJ and performance error. $e(n)$ and $r(n + m)$ denote the cyclical components of the performance error and rIMCJ normalized for each subject. The long-term trend components described by *Eqs.5* and *6* were presubtracted from the performance error and rIMCJ. Figure 8 shows cross-correlations between performance error and rIMCJ in the latter half of each movement duration, averaged across all subjects, and their 95% confidence intervals. Significant positive-correlation values were observed at the lags of one and two trials for the shoulder, and at the lag of two trials for the elbow. A positive correlation value for a positive time lag means a positive correlation between the performance error and subsequent rIMCJ, that is, a higher rIMCJ follows a poor performance, and a lower rIMCJ follows a good performance. For the elbow, we also found a significant negative correlation at zero lag, suggesting an instantaneous response of the performance error to the rIMCJ. The negative correlation values for zero lag indicated that the performance was good when the rIMCJ was high, while the performance was bad when the rIMCJ was low. The observed positive correlation values at lags of a few trials suggested the existence of short-term interactions between the viscoelasticity and performance error. These observations were found in the latter half of the movement duration but were not significant in the first half of the movement duration.

TABLE 1. *Correlation coefficients between the successful trial number and rIMCJ for each subject*

Subject	Shoulder	Elbow
Y.O.	−0.709**	−0.644**
K.D.	−0.660**	−0.486**
N.H.	−0.415**	−0.378**
H.S.	−0.442**	0.071 n.s.
Y.K.	0.175 n.s.	0.075 n.s.
Y.M.	−0.418**	−0.520**

** $P < 0.01$.
n.s., not significant: rIMCJ, index of muscle co-contraction around the joint.

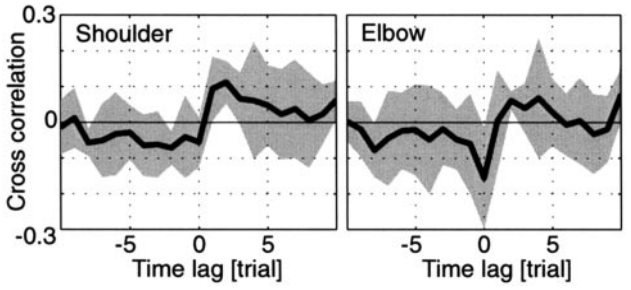

FIG. 8. Average cross-correlations between performance error and rIMCJ and their 95% confidence intervals, in the latter half of each movement duration, averaged across 6 subjects. Trend components were presubtracted from normalized values. A positive correlation value for a positive time lag means a positive correlation between the performance error and subsequent rIMCJ.

To further examine the properties of the interactions, we analyzed the time series data for each subject using the BMF statistical model described in *Eqs. 3–8* and in Fig. 2. The interactions between rIMCJ and performance error were examined for each subject by computing the impulse response of

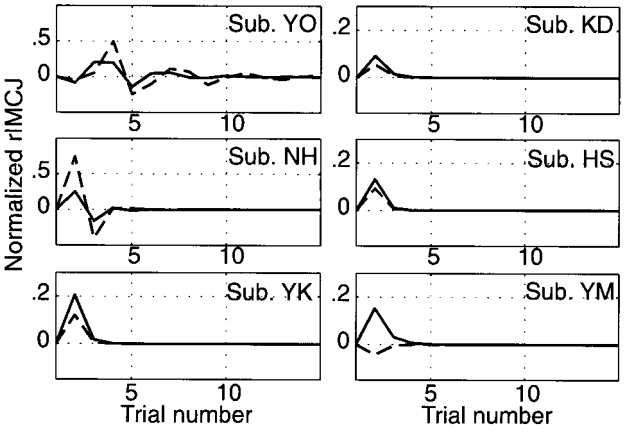

FIG. 9. Estimated response of rIMCJ when a performance error impulse was fed into the system for each subject. Solid curves denote estimates obtained from real data. Broken curves denote estimates obtained from simulated data generated by the Monte Carlo method (Marsaglia and Bray 1964). Both the real data and simulated data showed similar positive impulse responses for 5 of 6 subjects (subjects Y.O., K.D., N.H., H.S., and Y.K.), suggesting that the estimated performance error–rIMCJ interactions were reliable.

TABLE 2. *Maximum likelihood and AIC values for each AR order in cyclical components of measured and simulated data for subject Y.O.*

Measured Data		
AR Order	Maximum Likelihood	AIC
1	−173.185	362.369
2	−171.047	364.094
3	−167.591	363.182
4	−163.263	360.527
5	−162.038	364.075
Simulated Data		
AR Order	Maximum Likelihood	AIC
1	−169.350	354.700
2	−165.547	353.094
3	−150.505	329.009
4	−143.564	321.127
5	−143.249	326.499

AIC, Akaike's Information Criterion; AR, auto-regressive.

the system. To confirm the reproducibility of the model, we executed simulations by the Monte Carlo method (see APPENDIX 1). We processed only the rIMCJ values for the latter half of each movement duration, where significant cross-correlations were found.

Figure 9 shows the estimated response of the shoulder rIMCJ when a performance error impulse was input into the system. For five of six subjects, similar impulse responses were obtained from both real data and simulated data generated by the Monte Carlo method, suggesting that the observed transfer characteristics between the components were significant. That is, for these subjects, the shoulder rIMCJ showed a significant positive response to performance error input, which indicates that rIMCJ was positively correlated with the performance error levels in the immediately preceding trials. The results suggested that large performance errors will lead to a greater shoulder viscoelasticity, whereas small performance errors will lead to a lower viscoelasticity in subsequent trials. Interactions like these were not so obvious for the elbow rIMCJ and when the shoulder rIMCJ was restricted to the first half of each movement duration. Therefore previous performance mainly affected the viscoelasticity during the braking phase, and the shoulder viscoelasticity was more sensitive to this preceding performance than the elbow viscoelasticity.

The reproducibility of the estimated models and the reliability of the estimated values were examined from several aspects. Table 2 shows maximum likelihood and AIC values for each AR order in the cyclical components for subject Y.O. The top table shows the values when real data were used, while the bottom table shows the values when simulated data generated by the Monte Carlo method were used (see APPENDIX 1). In the case of this subject, an order of four (where the AIC value was minimal) was selected in the real data. The AIC value was again minimal at the order of four in the simulated data. The same AR order selected for both real data and simulated data demonstrates the reproducibility of an estimated model. All of the subjects here showed the same AR order for both the real data and simulated data. The AR order selected for subjects K.D., H.S., Y.K., and Y.M. was one, and for subject N.H., it was two. The reliability of the statistical model is described in APPENDIX 1.

DISCUSSION

IMCJ

We proposed a novel method for evaluating muscle co-contraction levels around the joint using surface EMG signals, and we confirmed that the values correspond well to the joint stiffness values in isometric contraction tasks as well as in dynamic tasks. The advantage of this method over the direct comparison of raw EMG signals, or EMG signals normalized by maximum voluntary contraction (MVC), is that the values have a physically meaningful unit. Because the magnitudes of raw EMG signals will change drastically for a number of reasons, such as the state of the electrodes, the distance between the electrodes, the configuration of muscles, skin condition, etc., they do not directly relate to a physical quantity, such as a force or stiffness. Even with MVC normalization, the contribution of each muscle is hard to assess. Therefore adding the raw EMG or normalized EMG of different muscles together has no physical meaning, because the weights among the multiple muscles are quite arbitrary. In contrast, in the present method, EMG signals are converted with reference to the generated joint torque so that they represent an absolute quantity. Because these converted values successfully represent a physically meaningful unit, they enable arithmetic operations such as addition and subtraction among operations of multiple muscles. This gives a measure for the net joint stiffness composed of multiple muscles as well as the relative contribution of each muscle to the joint stiffness. The present method can be used in a practical manner because the only requirement for computing the IMCJ is to measure the joint torque and surface EMG signals. Measuring the relationship between the joint torque and EMG is rather easy compared with that between the stiffness and EMG in terms of both mechanical and procedural demands (Osu and Gomi 1999).

Although the EMG-stiffness relationship during movements is quantitatively different from that during isometric contraction because of nonlinear components (such as length-tension or velocity-tension curves) or changes in moment arms according to the posture, the IMCJ successfully reproduced the relative change of joint co-contraction during movements (Fig. 4). The linear assumptions for force/velocity curves might have resulted in overestimating the agonist muscle torques compared with antagonist muscle torques. However, small errors in weighting antagonistic muscle pairs would not have severely affected the obtained results because none of the individual muscles showed a tendency distinctively opposite to the observed trend during learning. The assumption of constant moment arms is also over-simplified, especially for shoulder muscles. Pectoralis major moment arm might have changed 20% and posterior deltoid moment arm might have changed 30% for the movements examined here (Kuechle et al. 1997). Biceps and triceps moment arms seemed to be rather constant, while the brachioradialis moment arm might have changed 20–30% for the movements examined here (Murray et al. 1995). Such changes might have caused some error but would not have severely affected the results as long as we were observing almost identical trajectories within each subject, on the same day, and just looking at relative changes.

Even if the linearity assumption was wildly violated in reality, the proposed rather simple model and methods are still useful for the purpose of comparison and give us a better index for net joint stiffness than conventional normalization and summed EMG from multiple muscles. Previous estimation of dynamic torque and stiffness from EMG using a neural network model (Koike and Kawato 1995), and our recent estimation of dynamic stiffness from EMG signals with simultaneous measurements of stiffness by PFM, support the validity of using EMG signals for the stiffness estimation (Franklin et al. 2000). In summary, if torque levels are well corrected for movements, the present method is quite effective in assessing relative changes in the joint viscoelasticity during movements within a single subject.

Integration of internal model control and viscoelasticity

We observed a long-term decrease in rIMCJ in the learning of planar arm movements. The learning enabled the subjects to generate the same trajectory with less rIMCJ. The present work succeeded in observing pure changes in the viscoelastic force by requiring strict trajectory control and examining only successful trials. Such observations would be difficult in force-field learning (Milner and Cloutier 1993; Shadmehr and Mussa-Ivaldi 1994; Thoroughman and Shadmehr 1999), because force-fields severely perturb hand trajectories. Thoroughman and Shadmehr (1999) observed decreases in wasted contraction, that is, the amount of activation canceled by opposing muscles, in the learning of a novel force-field. However, wasted contraction does not necessarily reflect the viscoelasticity of the system. Even with a decrease in the wasted contraction, the increased effective contraction that compensates for the applied force-field can provide the necessary viscoelasticity to stabilize the movement. Accordingly, their findings do not directly demonstrate the change of weight on the viscoelastic force. By giving strict constraints on trajectories and comparing stiffness values among movements with similar trajectories, we were able to demonstrate the decrease of viscoelastic force for the first time.

Given that there is no change in the movement trajectory nor in the joint torque, the only possible explanation for the decrease in the viscoelastic forces (peripheral feedback control gain) is an increase in the contribution of the feedforward component (internal model control). When learning a new task, unpredictable dynamic forces acting on the multijoint links (e.g., interaction force, Coriolis force, or centrifugal force) might perturb the movements. As implicated by the equilibrium-point control hypothesis, viscoelastic force produced by both intrinsic muscle properties and spinal reflex will counteract such unpredictable perturbation (Flash 1987). As the learning proceeds, the CNS acquires the internal models that predict and generate necessary motor commands to compensate for the perturbation (Imamizu et al. 2000). The CNS weighs the viscoelastic force more strongly at the beginning of learning when the internal models are poor, and it gradually increases the internal model contribution as the learning proceeds. The short-term interaction between the performance error and rIMCJ suggests that the CNS actively regulates the viscoelasticity.

We propose an integration of the two theories, that is, the equilibrium-point control hypothesis and internal model–control hypothesis, on the assumption that learning improves the internal models (Fig. 10*A*). The final motor command is the summation of the parallel outputs from the "feedforward controller using the internal models" and "feedback controller supported by the viscoelasticity"; furthermore, the contribution of each output to the command is regulated by changing the peripheral feedback gain, that is, the magnitude of the viscoelastic force. The CNS monitors the improvement of the internal models and the performance. The CNS relies on the viscoelasticity when the internal models are imperfect or the environment is unstable, while it utilizes the internal models after they improve and the environment is stable (Fig. 10*B*). In addition to such long-term interactions, our findings further suggest short-term viscoelasticity-performance interactions on a trial-by-trial basis. If a movement is currently inaccurate, the contribution of the viscoelasticity is increased within several trials to improve the performance. If a movement is currently accurate, on the other hand, the contribution of the internal models is increased within several trials. Accordingly, the CNS can learn the internal models without loss of movement accuracy by using viscoelasticity-dependent control at the onset of learning and employing off-line feedback of the performance to regulate the viscoelasticity.

Such a strategy can be related to the common engineering technique of solving a problem by slowly shifting task parameters from domains where the solution is easy to domains where the solution is difficult (continuation method). In robot

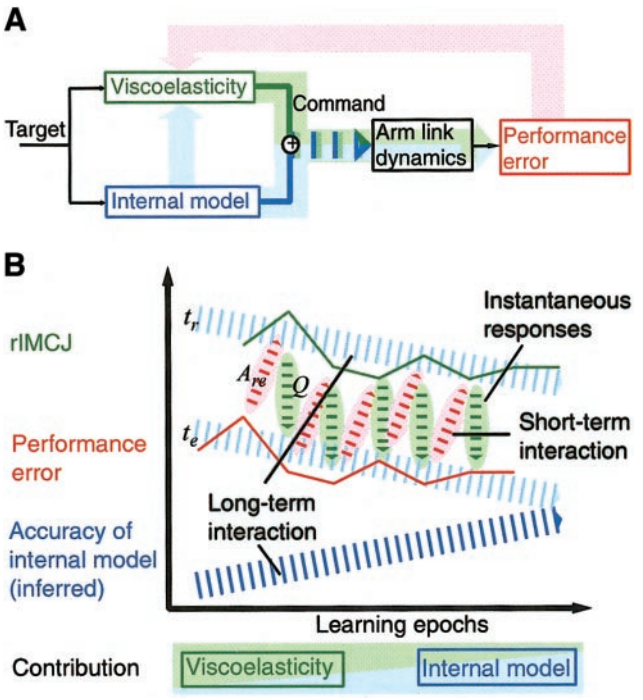

FIG. 10. *A*: integration of internal model control and viscoelasticity-dependent control. Thick green arrow shows that a high viscoelastic force instantaneously reduces the performance error. Thick red arrow shows that the performance error results in transient increases in viscoelastic forces in subsequent movements. Thick blue arrow shows that an improvement of the internal models results in gradual decreases in both viscoelastic forces and performance error. Summation of the output from these 2 control systems is the final motor command sent to the limbs. *B*: changes rIMCJ (green), performance error (red), and accuracy of the internal models (blue) associated with learning predicted by the integrated model. As the internal models improve, the output from the internal models increases.

learning, for example, higher learning rates were obtained by gradually increasing the speed or decreasing the stiffness as the learning progressed (Katayama et al. 1998; Sanger 1994). Behavioral studies have suggested that the internal models in the brain are relatively local in their generalization. They are accurate around previously learned trajectories but inaccurate for unexplored trajectories; the internal models are not parametric with a global generalization capacity (Gandolfo et al. 1996; Ghahramani et al. 1996; Imamizu et al. 1995; Kitazawa et al. 1997; Thoroughman and Shadmehr 2000). An internal model that achieves a novel desired trajectory cannot be acquired from those trajectories that differ greatly from the desired one. By sufficiently increasing the viscoelastic forces, however, trajectories around the desired one can be repetitively practiced, even at the onset of learning. An increased viscoelastic force at the onset of learning is also effective in learning schemes that utilize motor command errors read from the feedback controller as learning signals for internal models (Kawato et al. 1987, 1993).

Active and predictive control of viscoelastic force

Whether the CNS actually regulates the joint viscoelasticity or whether this parameter is simply an incidental by-product of the overlapping activity of agonist and antagonist muscles has remained an unsettled problem (Gomi 1996; Smith 1996; Thoroughman and Shadmehr 1999; Van Galen et al. 1996). The present results showed that performance error can explain future rIMCJ, especially in the shoulder, during deceleration; this supports the idea that the CNS actively and predictively controls the viscoelasticity. Viscoelasticity regulation by the off-line feedback of the performance may assist in learning movements. Such short-term interactions are not yet implemented in other biological models recently proposed, in which the feedforward compensation of the external force is parallel with the co-contraction mechanism to stabilize the movement (Flash and Gurevich 1997; Gribble and Ostry 2000; Katayama et al. 1998; Wang et al. 2001).

Van Galen and his colleagues (Van Galen and DeJong 1995; Van Galen and Schomaker 1992; Van Galen et al. 1990) hypothesized that stiffness control is an effective means of accuracy control. They stated that a high feedback gain will reduce the endpoint error. The CNS may increase the viscoelastic forces to execute more accurate movements. This is in good agreement with the present results, i.e., after unsuccessful trials, the rIMCJ increased to result in successful trials. Increases were more frequent in the latter half of each reaching movement duration, and this suggests the intention of the subjects to increase the endpoint accuracy.

The hypothesis that an increase in stiffness improves the endpoint accuracy, however, may appear to contradict the observed long-term decrease in rIMCJ. Although the rIMCJ was lower at the end of learning than at the beginning of learning, the accuracy of the movements increased significantly after extensive learning. This hypothesis of stiffness control may also be at odds with Harris and Wolpert (1998), because stiffness increases require larger motor commands, which in turn introduce higher levels of noise that causes larger trajectory errors. One explanation is that the CNS adopts dual strategies to improve the accuracy and chooses which strategy to use depending on the accuracy of the internal models. When the internal models are immature, the CNS tries to increase the viscoelastic force and utilizes muscles and neural feedback to compensate for unexpected interaction forces. Once an internal model is acquired, the CNS tries to decrease the motor command amplitude by decreasing the viscoelastic force, reducing the noise and increasing the accuracy. An increase in viscoelastic force is effective for a temporary increase in accuracy against perturbations; any muscle activation should be decreased to maintain a good performance over the long run.

We can think of several advantages in controlling an arm with low viscoelasticity: low muscle activation increases efficiency and prevents muscle fatigue, and a compliant limb reduces the potential for injury when it contacts an object in the environment. However, viscoelasticity is indispensable for stable control. Without viscoelasticity, spatiotemporal disturbances in the environment, such as objects to be manipulated, force-fields, or even changes in trajectories, can perturb limbs, resulting in instability. It therefore makes sense computationally to increase the limb compliance when moving in a stable environment, while adaptively increasing the viscoelastic force in response to instability in the environment (Lacquaniti et al. 1993). This study suggests that the CNS is equipped with an ingenious mechanism of learning and controlling movements, which regulates viscoelasticity on a short- and long-term basis, depending on performance error, and finally acquires smooth and accurate movements while maintaining stability during the entire learning process.

APPENDIX 1

Advantages of the BMF model

The BMF model has the following advantages.

1) Multivariate mean-nonstationary time-series data can be decomposed into its nonstationary trend components and other mutually related stationary cyclical components described by an AR model through one single procedure.

2) The AIC can be used to evaluate the accuracy of the decomposition.

3) The structure of the mutual relationships among the stationary cyclical components (e.g., impulse responses) can be derived from estimated AR coefficient matrices by applying system analysis techniques (Akaike and Nakagawa 1972; Kato and Kawahara 1998).

4) The reliability of the estimated parameters of the model can be confirmed by reapplying the system analysis to the simulated data sets, which are themselves generated based on the estimated model (Monte Carlo simulation).

Evaluation of the model

To examine the reproducibility of the estimated model, we generated data by using Gaussian noise as the system-noise input in the model estimated from the measured data (the Monte Carlo method), and re-estimated the model parameters by fitting the AR model to the simulated data. Examining empirical data generated through Monte Carlo simulation is an effective way of investigating the properties and reproducibility of such a model, especially when samples are limited and it is impossible to get another data set to test the model (Lutkepohl 1993). Actually, simulated data can be produced by applying artificially generated Gaussian white noise as input to the noise components of the model estimated from the measured data. If the assumptions about the whiteness and Gaussian distribution of the noise are satisfied, the simulated data should reflect the stochastic characteristics of the measured data. If the assumptions are not ade-

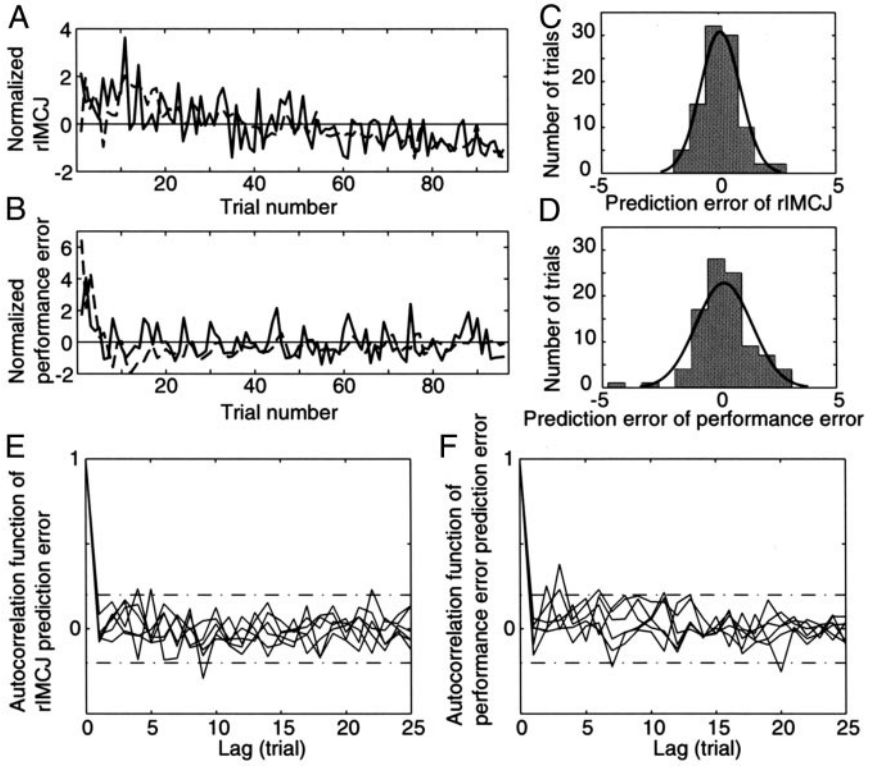

FIG. A1. *A* and *B*: predictability of (*A*) rIMCJ and (*B*) performance error for 1 typical subject (subject Y.O.) using the model. Plots show normalized data (solid curves) and 1-step predictions (dashed curves) calculated from the proposed statistical model. *C* and *D*: distribution of prediction errors for (*C*) rIMCJ and (*D*) performance error with fitted Gaussian curves for subject Y.O. *E* and *F*: autocorrelation function of prediction error for (*E*) rIMCJ and (*F*) performance error with the 95% confidence interval (dash-dot lines) for 6 subjects.

quate, the white Gaussian noise input will not be able to simulate the measured data. Therefore by reapplying the same system-analysis procedure to the simulated data, we checked whether the simulated data had physiological properties identical to the measured data. Similar estimation results obtained from both the measured and simulated data sets verified the adequacy of the estimators, and at the same time, the assumption of the white Gaussian noise. In our simulation, Gaussian random numbers were computed using the Marsaglia method (Marsaglia and Bray 1964) and input to each noise component of the model. The parameters were again estimated by fitting the BMF model to the simulated data. Impulse responses were computed from the parameters obtained by the simulation data and compared with the impulse responses obtained from the real data. Similar impulse responses and the same AR order obtained from both real data and the simulated data set confirm the validity of the model and the estimators (Fig. 9 and Table 2).

Figure A1, *A* and *B*, shows the prediction capability of the model for the (*A*) rIMCJ and (*B*) performance error for subject Y.O. The solid curves denote normalized data and the dashed curves denote one-step predictions computed from the proposed statistical model. The one-step predictions demonstrate the predictive part of the model described as an auto-regressive form by *Eqs. 7* and *8*. Differences between one-step predictions and the data (prediction error) demonstrate the stochastic nature of the system, mainly described by the system noise $\varepsilon_r(n)$ and $\varepsilon_e(n)$ in *Eqs. 7* and *8*. A similarity of a one-step prediction with the data demonstrates the predictability of the model (goodness of fit), although they did not perfectly fit one another because of the stochastic nature of the system.

As mentioned above, in deriving the properties of the estimators, white Gausssian noise was assumed as the system noise input to the model. If the assumed model were appropriate, the interactions would be fully extracted by the model and only the stochastic components would remain as the prediction error. In this case, if the BMF model structure and estimated model parameters are appropriate, the prediction error should be white and Gaussian as assumed. On the other hand, if the assumed model were poor or inappropriate to describe the underlying system, the interactions that could not be modeled would appear in the prediction error. We confirmed the validity of the assumption by an autocorrelation function and the distribution of prediction errors. Figure A1, *C* and *D*, shows distributions of prediction error for the same subject. The observed normally distributed prediction error demonstrated that the Gaussian noise assumption was satisfied by the data. All of the other subjects showed similar Gaussian distributions of prediction error. Figure A1, *E* and *F*, shows autocorrelations of the prediction error for all subjects. The dash-dot lines denote 95% confidence intervals. The lack of correlations at lags >0 demonstrates that the assumption of the whiteness of the noise was also satisfied. The white and Gaussian prediction errors observed for all subjects confirmed the validity of the assumed model and the reliability of the estimated parameters and impulse responses.

APPENDIX 2

The details of dynamic stiffness estimation and IMCJ computation

For estimation of dynamic stiffness and corresponding dynamic IMCJ, the subject performed a series of reaching movements while coupled to the PFM. The right forearm of the subject was firmly attached to the PFM using a molded plastic cuff. The cuff immobilized the wrist joint, permitting movement only at the shoulder and elbow. The right forearm was supported on a beam fixed to the handle of the PFM. The subject performed a reaching movement from a start target (located 31 cm in front of the shoulder) to an end target (located 56 cm in front of the shoulder). The subject was required to produce movements of 600 ± 100 ms duration. The force-fields applied were null force-field, velocity-dependent force-field $\left(\begin{bmatrix} F_x \\ F_y \end{bmatrix} = \alpha \begin{bmatrix} 13 & -18 \\ 18 & 13 \end{bmatrix} \begin{bmatrix} \dot{x} \\ \dot{y} \end{bmatrix}\right)$, and position-dependent force-field $\left(\begin{bmatrix} F_x \\ F_y \end{bmatrix} = \begin{bmatrix} \beta x \\ 0 \end{bmatrix}\right)$. Here α and β were chosen depending on the subject's force ($\frac{2}{3} \leq \alpha \leq 1$; $300 \leq \beta \leq 500$). The endpoint stiffness of the arm was determined by applying displacement in each of eight directions during the mid-portion of a movement. The

displacement onset occurred 150 ms after the movement onset. Eighty trials without displacement were randomly intermingled with the displacement trials for a total of 160 trials. The details of the stiffness estimation and the experimental setup are presented elsewhere (Burdet et al. 2000, 2001). The endpoint stiffness was converted to joint stiffness. At the same time, EMG signals were recorded from six arm muscles. The EMG signals of 80 trials without displacement were rectified and averaged for each muscle for a period of 300 ms during the mid-portion of a movement, including the portion where the perturbations were applied in the displacement trials. The means over 80 no-displacement trials were used to compute shoulder and elbow IMCJs.

We thank Dr. Y. Tohkura of Nippon Telegraph and Telephone Corporation for continuing encouragement, and Dr. T. E. Milner of Simon Fraser University for improving the manuscript.

This work was supported by the Human Frontier Science Program, the Special Coordination Fund to Brain Science, and the Telecommunications Advancement Organization of Japan.

REFERENCES

AKAIKE H. A new look at the statistical identification. *IEEE Trans Automat Control* 19: 716–723, 1974.

AKAIKE H AND NAKAGAWA T. *Statistical Analysis and Control of Dynamics Systems.* Tokyo, Japan: Scientific Publishers, 1972.

BASMAJIAN JV AND DE LUCA CJ. *Muscles Alive.* Baltimore, MD: Williams and Wilkins, 1985.

BENNETT DJ, HOLLERBACH JM, XU Y, AND HUNTER IW. Time-varying stiffness of human elbow joint during cyclic voluntary movement. *Exp Brain Res* 88: 433–442, 1992.

BERNSTEIN N. *The Coordination and Regulation of Movements.* Oxford: Pergamon Press, 1967.

BIZZI E, ACCORNERO N, CHAPPLE W, AND HOGAN N. Posture control and trajectory formation during arm movement. *J Neurosci* 4: 2738–2744, 1984.

BIZZI E AND MUSSA-IVALDI FA. Neural basis of motor control and its cognitive implications. *Trends Cog Sci* 2: 97–102, 1998.

BURDET E, OSU R, FRANKLIN DW, MILNER TE, AND KAWATO M. The central nervous system stabilizes unstable dynamics by learning optimal impedance. *Nature* 414: 446–449, 2001.

BURDET E, OSU R, FRANKLIN DW, YOSHIOKA T, MILNER TE, AND KAWATO M. A method for measuring endpoint stiffness during multi-joint arm movements. *J Biomech* 33: 1705–1709, 2000.

FELDMAN AG. Functional tuning of nervous system with control of movement or maintenance of a steady posture. 2. Controllable parameters of the muscles. *Biophysics* 11: 565–578, 1966.

FLANAGAN JR, OSTRY DJ, AND FELDMAN AG. Control of trajectory modifications in target-directed reaching. *J Mot Behav* 25: 140–152, 1993.

FLASH T. The control of hand equilibrium trajectories in multi-joint arm movements. *Biol Cybern* 57: 257–274, 1987.

FLASH T AND GUREVICH I. Arm trajectory generation and stiffness control during motor adaptation to external loads. In: *Self-Organization, Computational Maps and Motor Control*, edited by Morasso PG and Sanguinetti V. Amsterdam: Elsevier, 1997, p. 423–482.

FRANKLIN DW, OSU R, BURDET E, KAWATO M, AND MILNER TE. Learning to stabilize unstable dynamics: III. EMG correlates. *Soc Neurosci Abst* 26: 171, 2000.

GANDOLFO F, MUSSA-IVALDI FA, AND BIZZI E. Motor learning by field approximation. *Proc Natl Acad Sci USA* 93: 3843–3846, 1996.

GHAHRAMANI Z, WOLPERT DM, AND JORDAN MI. Generalization to local remappings of the visuomotor coordinate transformation. *J Neurosci* 16: 7085–7096, 1996.

GOMI H. Is stiffness a byproduct or a target? *Behav Brain Sci* 19: 450–451, 1996.

GOMI H AND KAWATO M. Task dependent stiffness of human multi-joint arm during point-to-point movement. *NTT Basic Res Labs Inform Sci Res Lab*, ISRL-95-104, 1995.

GOMI H AND KAWATO M. Equilibrium-point control hypothesis examined by measured arm stiffness during multijoint movement. *Science* 272: 117–120, 1996.

GOMI H AND KAWATO M. Human arm stiffness and equilibrium-point trajectory during multi-joint movement. *Biol Cybern* 76: 163–171, 1997.

GOMI H AND OSU R. Task-dependent viscoelasticity of human multijoint arm and its spatial characteristics for interaction with environments. *J Neurosci* 18: 8965–8978, 1998.

GRIBBLE PL AND OSTRY DJ. Compensation for loads during arm movements using equilibrium-point control. *Exp Brain Res* 135: 474–482, 2000.

GRIBBLE PL, OSTRY DJ, SANGUINETI V, AND LABOISSIERE R. Are complex control signals required for human arm movement? *J Neurophysiol* 79: 1409–1424, 1998.

HARRIS CM AND WOLPERT DM. Signal-dependent noise determines motor planning. *Nature* 394: 780–784, 1998.

HOGAN N. An organizing principle for a class of voluntary movements. *J Neurosci* 4: 2745–2754, 1984.

HUNTER IW AND KEARNEY RE. Dynamics of human ankle stiffness: variation with mean ankle torque. *J Biomech* 15: 747–752, 1982.

IMAMIZU H, MIYAUCHI S, TAMADA T, SASAKI Y, TAKINO R, PUTZ B, YOSHIOKA T, AND KAWATO M. Human cerebellar activity reflecting an acquired internal model of a new tool. *Nature* 403: 192–195, 2000.

IMAMIZU H, UNO Y, AND KAWATO M. Internal representations of the motor apparatus: implications from generalization in visuomotor learning. *J Exp Psychol Hum Percept Perform* 21: 1174–1198, 1995.

ISHIGURO M AND AKAIKE H. *DALL: Davidon's Algorithm for Log Likelihood Maximization.* Tokyo: The Institute of Statistical Mathematics, 1989.

ISHIGURO M, KATO H, AND AKAIKE H. *Ardock: An Auto-Regressive Model Analyzer.* Tokyo: The Institute of Statistical Mathematics, 1999.

KATAYAMA M, INOUE S, AND KAWATO M. A strategy of motor learning using adjustable parameters for arm movement. *Proc 20th Annu Int Conf IEEE Eng Med Biol Soc*, 1998, p. 2370–2373.

KATAYAMA M AND KAWATO M. Virtual trajectory and stiffness ellipse during multi-joint arm movement predicted by neural inverse models. *Biol Cybern* 69: 353–362, 1993.

KATO H AND KAWAHARA H. An application of the Bayesian time series model and statistical system analysis for F0 control. *Speech Commun* 24: 325–359, 1998.

KAWATO M, FURUKAWA K, AND SUZUKI R. A hierarchical neural-network model for control and learning of voluntary movement. *Biol Cybern* 57: 169–185, 1987.

KAWATO M, GOMI H, KATAYAMA M, AND KOIKE Y. Supervised learning for coordinative motor control. In: *Computational Learning and Cognition, SIAM Frontier Series*, edited by Baum EB. Philadelphia, PA: Society for Industrial and Applied Mathematics, 1993, p. 126–161.

KITAZAWA S, KIMURA T, AND UKA T. Prism adaptation of reaching movements: specificity for the velocity of reaching. *J Neurosci* 17: 1481–1492, 1997.

KOIKE Y AND KAWATO M. Virtual trajectories predicted from surface EMG signals. *Soc Neurosci Abstr* 19: 543, 1993.

KOIKE Y AND KAWATO M. Estimation of dynamic joint torques and trajectory formation from surface electromyography signals using a neural network model. *Biol Cybern* 73: 291–300, 1995.

KUECHLE DK, NEWMAN SR, ITOI E, MORREY BF, AND AN KN. Shoulder muscle moment arms during horizontal flexion and elevation. *J Shoulder Elbow Surg* 6: 429–439, 1997.

LACKNER JR AND DIZIO P. Rapid adaptation to Coriolis force perturbations of arm trajectory. *J Neurophysiol* 72: 299–313, 1994.

LACQUANITI F, CARROZZO M, AND BORGHESE NA. Time-varying mechanical behavior of multijointed arm in man. *J Neurophysiol* 69: 1443–1464, 1993.

LATASH ML AND GOTTLIEB GL. Reconstruction of shifting elbow joint compliant characteristics during fast and slow movements. *Neuroscience* 43: 697–712, 1991.

LUTKEPOHL H. *Introduction to Multiple Time Series Analysis.* Berlin: Springer-Verlag, 1993.

MARSAGLIA G AND BRAY TA. A convenient method for generating normal variables. *SIAM Review* 6: 260–264, 1964.

MIALL RC, WEIR DJ, WOLPERT DM, AND STEIN JF. Is the cerebellum a Smith predictor? *J Motor Behavior* 25: 203–216, 1993.

MILNER TE AND CLOUTIER C. Compensation for mechanically unstable loading in voluntary wrist movement. *Exp Brain Res* 94: 522–532, 1993.

MURRAY WM, DELP SL, AND BUCHANAN TS. Variation of muscle moment arms with elbow and forearm position. *J Biomech* 28: 513–525, 1995.

MUSSA-IVALDI FA, HOGAN N, AND BIZZI E. Neural, mechanical, and geometric factors subserving arm posture in humans. *J Neurosci* 5: 2732–2743, 1985.

NAKANO E, IMAMIZU H, OSU R, UNO Y, GOMI H, YOSHIOKA T, AND KAWATO M. Quantitative examinations of internal representations for arm trajectory planning: minimum commanded torque change model. *J Neurophysiol* 81: 2140–2155, 1999.

OSU R AND GOMI H. Multi-joint muscle regulation mechanisms examined by measured human-arm stiffness and EMG signals. *J Neurophysiol* 81: 1458–1468, 1999.

POLLICK FE AND ISHIMURA G. The three-dimensional curvature of straight-ahead movements. *J Motor Behavior* 28: 271–279, 1996.

SANGER TD. Neural network learning control of robot manipulators using gradually increasing task difficulty. *IEEE Trans Robotics Automat* 10: 323–333, 1994.

SHADMEHR R AND MUSSA-IVALDI FA. Adaptive representation of dynamics during learning of a motor task. *J Neurosci* 14: 3208–3224, 1994.

SHIDARA M, KAWANO K, GOMI H, AND KAWATO M. Inverse-dynamics model eye movement control by Purkinje cells in the cerebellum. *Nature* 365: 50–52, 1993.

SMITH A. Does the cerebellum learn strategies for the optimal time-varying control of joint stiffness? *Behav Brain Sci* 19: 399–410, 1996.

THOROUGHMAN KA AND SHADMEHR R. Electromyographic correlates of learning an internal model of reaching movements. *J Neurosci* 19: 8573–8588, 1999.

THOROUGHMAN KA AND SHADMEHR R. Learning of action through adaptive combination of motor primitives. *Nature* 407: 742–747, 2000.

VAN GALEN GP AND DEJONG WP. Fitts' law as the outcome of a dynamic noise filtering model of motor control. *Hum Mov Sci* 14: 539–571, 1995.

VAN GALEN GP, HENDRIKS AW, AND DEJONG WP. What behavioral benefit does stiffness control have? An elaboration of Smith's proposal. *Behav Brain Sci* 19: 478–479, 1996.

VAN GALEN GP AND SCHOMAKER LRB. Fitts' law as a low-pass filter effect of muscle stiffnesss. *Hum Mov Sci* 11: 11–21, 1992.

VAN GALEN GP, VAN DOORN RR, AND SCHOMAKER LR. Effects of motor programming on the power spectral density function of finger and wrist movements. *J Exp Psychol Hum Percept Perform* 16: 755–765, 1990.

WANG T, DORDEVIC GS, AND SHADMEHR R. Learning the dynamics of reaching movements results in the modification of arm impedance and long-latency perturbation responses. *Biol Cybern* 85: 437–448, 2001.

WINTERS JM. Hill-based muscle models: a systems engineering perspective. In: *Multiple Muscle Systems*, edited by Winters JM and Woo SL-Y. New York: Springer-Verlag, 1990, p. 69–93.